Full-Duplex mmWave Radio-over-Fiber Architecture with Simplified Photonic Frequency Translation

Bernhard Schrenk, *Member, IEEE*, and Fotini Karinou, *Senior Member, IEEE*

***Abstract*—Fiber-optics plays a critical role for the deployment of beyond-5G networks. Towards this direction, we will evaluate simplified remote radio head optics based on an electro-absorption modulated laser that is operated as a full-duplex mm-wave transceiver. We experimentally show, for the first time, that the coherent homodyne reception methodology of our transceiver can inherently provide a transparent optical frequency translation of the radio signal, and prove this function through photonic up-/down-conversion of a down-/uplink signal between the K_a-band and a low radio carrier frequency. We will experimentally confirm these points through full-duplex radio transmission at 34.3/29.3 GHz over an optical budget of 18.7 dB and a reach of 15 km. The proposed scheme is found to reduce the overall complexity of the mobile fronthaul link through a reduction in the required high-frequency mixers and synthesizers, while further enhancing the robustness of the mm-wave radio-over-fiber transmission to dispersion-induced fading.**

***Index Terms*—Optical communication terminals, Optical signal detection, 6G mobile communication**

I. INTRODUCTION

ELEVATED radio carrier frequencies, lower latency, higher reliability and cell-free architectures that heterogeneously blend with beam-centric small-cell radio schemes are considered the cornerstones of beyond-5G radio networks [1]. Out of this quiver of advancements, the ~10-fold increase in radio frequency (RF) can be seen as the most disruptive enhancement as it enables the introduction of beamforming concepts while significantly boosting the per-user date rate. Since antenna remoting through radio-over-fiber (RoF) technology prevails as a way to centralize complex radio processors, the optically hauled radio access network architecture has to cater for the needs of transparently transporting macro- and small-cell signals. While the former are typically located in the sub-6GHz band and mostly supported by robust transmission involving the Common Public Radio Interface (CPRI) [2], the small cells are fed by quadrature amplitude modulated (QAM) orthogonally frequency division multiplexed (OFDM) radio signals [3-5] on (sub-)millimeter wave radio carriers. Both types of radio signals are being relayed between the central office (CO) and remote radio heads (RRH). At the same time, a minimum of complexity shall apply for the involved RoF sub-systems and the small-cell RRH in particular [6]. The latter is emphasized by the nature of the RRH as cost-sensitive, field-distributed network element that eludes itself from experiencing any pooling gain as it would apply for centralized sub-systems.

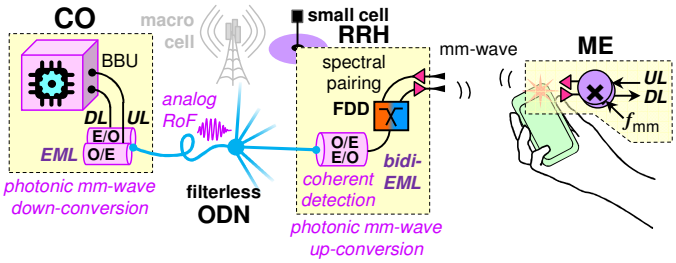

Fig. 1. Fronthaul architecture with photonic up- and down-conversion at RRH and CO, accomplished through EML-based opto-electronic radio signal converters.

This work extends our investigation [7] on the advancement of coherent analogue RoF transmission to the mm-wave band. We will demonstrate the use of an electro-absorption modulated laser (EML) not solely as full-duplex transceiver for K_a-band radio signals (Fig. 1); We will further show that the same EML can accomplish a radio-transparent optical frequency translation of the mm-wave radio signals from and to a much lower radio carrier.

This paper is organized as follows. Chapter II compares the proposed concepts for radio signal frequency translation to the state of the art. Chapter III introduces the experimental arrangement for evaluating our optoelectronic transceivers. Chapter IV discusses the radio signal transmission performance. Finally, Chapter V concludes the work.

II. RADIO-TRANSPARENT PHOTONIC FREQUENCY TRANSLATION IN FULL-DUPLEX TRANSCEIVERS

A. Photonic Up-Conversion

Photonic up-conversion simplifies the downlink radio transmission by substituting RF-based frequency translation by photonic means. Remarkable work has been done in this field, aiming at RF carrier frequencies up to the THz band [8].

There are two well-adopted approaches to obtain photonic up-conversion for a radio signal, as sketched in Fig. 2 and exemplified through Table I. The first relies on dedicated modulators and modulation schemes and tailors the (complex) optical spectrum during the transfer of a data signal from the

Manuscript received November 8, 2023. This work was supported in part by the European Research Council (ERC) under the European Union's Horizon 2020 research and innovation programme (grant agreement No 804769).

B. Schrenk is with the AIT Austrian Institute of Technology, Center for Digital Safety&Security, Giefinggasse 4, 1210 Vienna, Austria (phone: +43 50550-4131; fax: -4150; e-mail: bernhard.schrenk@ait.ac.at).

F. Karinou is with Microsoft Research Ltd, Cambridge, CB4 0GW, United Kingdom (e-mail: fotini.karinou@microsoft.com).

TABLE I
STATE-OF-THE-ART DEMONSTRATIONS FOR PHOTONIC UP- AND DOWN-CONVERSION

up / down	Ref.	*f* range [GHz]	Data format	Frequency-conversion technique	Complexity	Fronthaul architecture
Photonic up-conversion	[9]	9 → 36	sinusoidal tone	second-order harmonic generation + optical carrier suppression	dual-parallel, dual-electrode MZM	RF over fiber, high-speed PD at RRH
	[10]	36	0.75 Gb/s OOK	double-sideband modulation + optical carrier suppression	MZM biased at minimum	RF over fiber, high-speed PD at RRH
	[11]	28	1 GHz 16-QAM OFDM	independent sideband modulation	I/Q modulator	RF over fiber, high-speed PD at RRH
	[13]	47.3	6 Gbaud 16-QAM	dual-λ source with phase-locked spectral carriers	quantum-dash laser + line-selective I/Q modulation, EDFA booster at RRH	RF over fiber, high-speed PD at RRH
	[14]	300	30 Gbaud PAM4	heterodyne beating with free-running LO	low-linewidth (100 kHz) laser sources, EDFA booster at RRH, UTC-PD	Baseband data + LO over fiber, high-speed PD at RRH
	[15]	450	6.5 Gbaud QPSK	heterodyne beating with free-running external cavity laser	low-linewidth (<100 kHz) laser source, EDFA booster at RRH, UTC-PD	Baseband data + LO over fiber, high-speed PD at RRH
	[16]	320	50 Gb/s 16-QAM	heterodyne beating with free-running external cavity laser	I/Q modulator, low-linewidth (<100 kHz) laser source, EDFA booster at RRH, UTC-PD	Baseband data + LO over fiber, high-speed PD at RRH
	[17]	117	57.2 Gb/s 4096-QAM OFDM	heterodyne beating with free-running external cavity laser	I/Q modulator, low-linewidth laser source, UTC-PD	Baseband data + LO over fiber, high-speed PD at RRH
	[18]	92.5	15.7 Gbaud QPSK	heterodyne beating with free-running external cavity laser	low-linewidth laser source, UTC-PD	Baseband data over fiber, LO + high-speed PD at RRH
	[19]	360 - 430	25.8 Gbaud QPSK	heterodyne beating with free-running external cavity laser	low-linewidth (<100 kHz) laser source, UTC-PD	Baseband data over fiber, LO + high-speed PD at RRH
	[20]	28.1	10 Gbaud QPSK	heterodyne beating with free-running external cavity laser	low-linewidth (100 kHz) laser sources, dual-drive MZM, optical 90° mixer for up-conversion	Baseband data over fiber, LO + optical 90° mixer + high-speed PD at RRH
Photonic down-conversion	[24]	8.8 → 1.5	200 MHz linearly chirped signal	mixing uplink RF signal and RF LO in dual-parallel MZM with carrier-suppressed modulation	uplink detector with full RF bandwidth, dual-polarization dual-parallel MZM	no all-optical conversion: RF signal as electrical drive for dual-parallel MZM
	[25]	5.3…17.3 → 0.6	sinusoidal tone	beating of a comb modulated by uplink RF signal with a second comb used as LO	uplink detector with full RF bandwidth, two independent comb generators, low-bandwidth balanced detector	no all-optical conversion: RF signal as electrical drive for modulating comb
	[26]	11 → 1	sinusoidal tone	re-modulate RF signal by RF LO with dual-polarization dual-parallel MZM + polarization-domain image-reject detection	RF LO source, dual-polarization dual-parallel MZM, polarization tracking	suitable for RoF transmission as RFoF uplink signal
both	*this work*	14.25 → 30 29.3 → 3.5	0.5 GHz 16-QAM OFDM	homodyne detection through injection locking on virtual carrier + independent sideband modulation for up-conversion	EML as coherent homodyne detector, I/Q modulator for independent sideband modulation (only for up-conversion)	RF over fiber, single bidi EML at RRH

electrical to the optical domain. Examples for this category can be found in the suppression of the optical carrier [9, 10] or independent sideband modulation through a full-field inphase/quadrature (I/Q) modulator [11]. Depending whether or not data is modulated at both sidebands, the delivered radio power or the beat interference noise can be optimized as a system parameter [12]. In all these cases, where up-conversion takes place at the single-wavelength level, the corresponding RRH architecture remains greatly simplified, as it principally requires only a high-speed photodetector to translate the RoF signal into a higher-band RF signal before wireless transmission.

Alternatively, the photonic up-conversion can be accomplished by heterodyning an optical baseband data signal with an independent optical carrier generated by a free-running laser source. This local oscillator (LO), whose spectral detuning to the data signal will determine the RF carrier frequency, can be either placed at the CO [13-17] or directly at the RRH [18-20]. In the former case the optical budget of the fronthaul link will generally restrict the optical power of the LO that is available to the photodetector at the RRH. It is likely that the complexity of the cost-sensitive RRH is therefore increased by a local optical amplifier (OA) serving as signal booster [13-15]. On the other hand, the latter case that involves an LO at the RH necessitates the stable operation of a low-linewidth laser that is carefully fine-tuned to obtain the desired spectral detuning to the data signal (i.e. its resulting RF carrier frequency). This is to be accomplished at the environmentally exposed location of the field-distributed RRH, where no pooling gain towards an efficient wavelength management can be harvested, such as it would apply at the CO. Therefore, both heterodyning schemes unequivocally increase the complexity of the RRH. On top of this, the free-running LO remains asynchronous to the optical carrier of the data signal. Considering the end-to-end radio signal chain, this calls for costly low-linewidth sources and digital signal processing (DSP) based phase-noise compensation after radio reception [15-20], unless real-valued optical signals are employed in combination with envelope detection [14]. An elegant solution to mitigate this additional overhead in terms of complexity can be found in dual-wavelength sources, which generate phase-synchronous optical carriers for data modulation and up-conversion LO [13].

In contrast to the aforementioned schemes, our approach adopts an EML as demarcation point between the optical fronthaul and the mm-wave RF interfaces at the RRH (Fig.

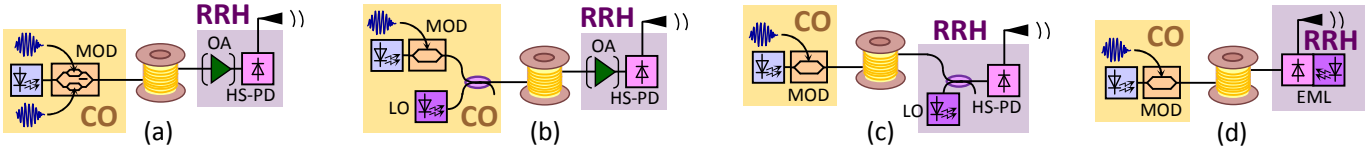

Fig. 2. Up-conversion through (a) modulation tailoring, (b) coherent beating with local and (c) remote LO, or (d) within an EML.

2(d)). The EML will serve as a coherent homodyne frequency translator between the optical (194.8 THz) and RF (K_a-band) domains. While the electro-absorption modulator (EAM) inherently generates a photocurrent, its distributed feedback (DFB) laser provides the optical reference that is required for coherent detection [21]. The advantage of this method is three-fold: First, the frequency of the RF downlink signal is preserved by virtue of a frequency-synchronized optical LO. This is accomplished by injection-locking the EML to the received downlink signal. Second, the co-integration of the DFB laser – as LO – and the EAM – as high-speed photodiode – results in phase-locked signal detection, thus enabling analogue RoF transmission without further DSP to address coherent detection impairments. Third, we will not restrict ourselves to lock the EML on the optical carrier Λ of the downlink signal; We will demonstrate that a virtual carrier (VC) inscribed to the data signal can serve as a spectral reference to which the LO is relating its optical emission frequency. With this, we accomplish a radio-transparent frequency translation without adding further complexity to the up-converting receiver. It shall be stressed that the EML located at the RRH would be subject to strong temperature fluctuations, which impact its emission frequency in case that an uncooled device is being employed. Given the tuning coefficient of 13.8 GHz/°C at an operating temperature of 40°C for the EML device used in this work, a detuning of up to 10 nm can be inferred under worst-case conditions. This would necessitate a widely yet slowly tunable EML solution to mitigate the impact of temperature fluctuations, such as provided through a laser with distributed Bragg reflector (DBR) section [22].

A representative spectral layout for the frequency translation process is presented in Fig. 3. The downlink (DL) transmitted by the CO (*R*), which is characterized by its optical carrier Λ and the RF carrier frequency f_{DL}, locks the LO at the RRH, which also becomes the optical carrier of the uplink (UL). Depending on the received optical power (ROP) of the downlink, a certain locking range (LR) applies for the EML receiver. Within this LR, frequency- and phase-synchronization can be guaranteed. EMLs have been characterized to feature a LR of 100 MHz for a ROP as low as -35 dBm [23]. Since the LR at low ROP is wide enough in view of the residual spectral drift of thermally stabilized sources, we can support a weak VC power, as will be proven in Section IV.

While Fig. 3 (*R*) presents the case for an RF up-converted downlink signal that is transmitted at its target carrier frequency f_{DL}, photonic up-conversion can be accomplished by locking on a VC at f_Λ, replacing the optical carrier Λ and, following the notion of an up-conversion, being allocated to

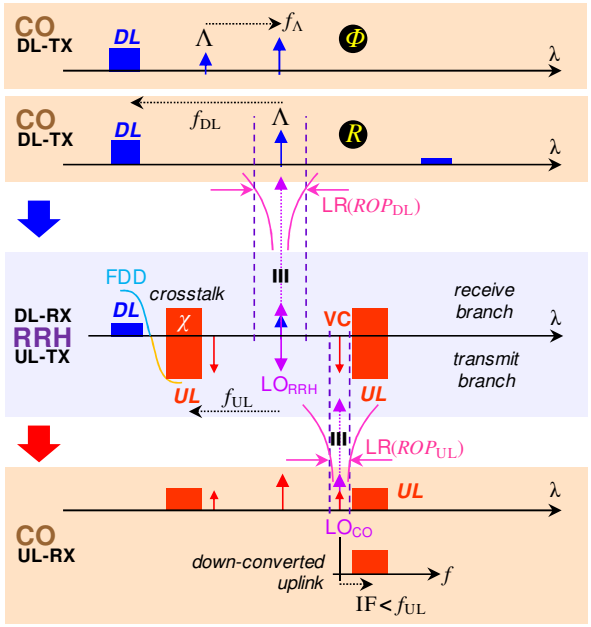

Fig. 3. Spectral allocation of downlink (DL), uplink (UL), LOs and VC for photonic frequency translation at RRH and CO.

the modulation sideband at the opposite side of Λ, in reference to the sideband including the downlink signal. For the sake of completeness, this case is represented as *Φ* in Fig. 3.

B. Photonic Down-Conversion

The reverse frequency translation process from a high RF to a much lower intermediate frequency (IF) poses a bigger challenge. Here, a considerably fewer number of works have primarily proven this functionality in its principle, at rather moderate RF frequencies (Table I). Moreover, most of the works, which primarily originate from the field of satellite communications, rely on the availability of the RF signal in the electrical domain, to directly apply it as drive signal for a modulator as part of the photonic down-converter [24, 25]. A more transparent scheme [26] that is suitable for uplink RoF transmission in mobile fronthaul networks avoids this o/e/o conversion of the RF signal by re-modulating it with an additional LO signature; However, the LO drive is subject to a similarly high frequency within the RF band of the signal that is to be down-converted, so that the complexity is just partially reduced. All of the aforementioned works rely on complex modulators that are further subject to high optical loss.

Our proposed approach again relies on the locking of the coherent homodyne receiver to a spectral line, which in the case of photonic down-conversion is taking shape as distinct VC that is embedded in close proximity to the uplink data signal at the RF carrier frequency f_{UL}. Figure 3 exemplifies such a scenario where the LO of the EML-based receiver at

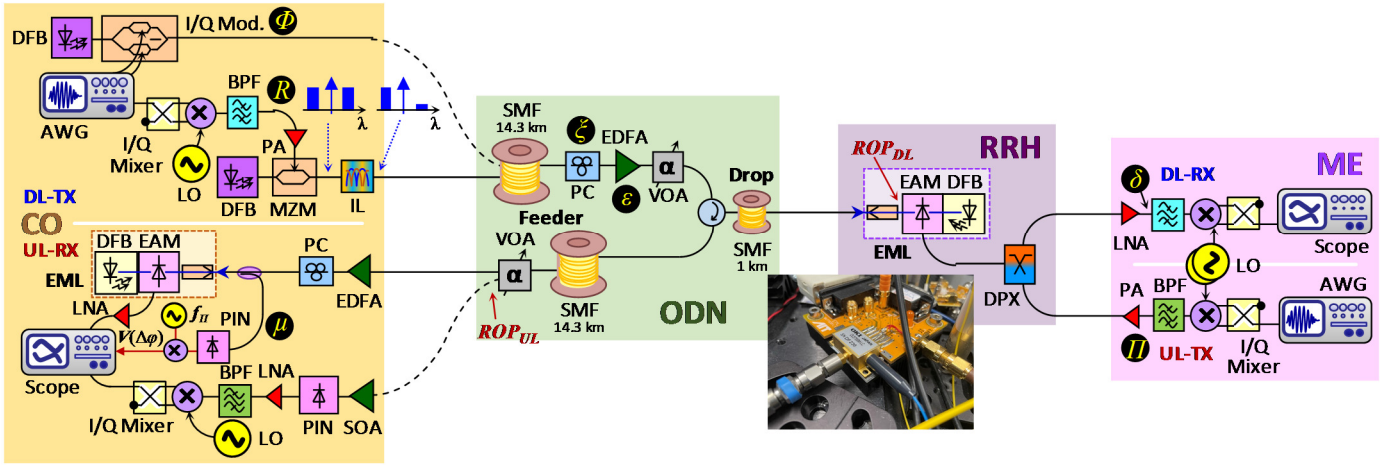

Fig. 4. Experimental setup. The inset shows the butterfly EML used as full-duplex opto-electronic signal converter at the RRH.

the CO locks onto the VC embedded with the uplink signal. Due to the large frequency difference, the optical uplink carrier, which is equivalent to the LO of the RRH at Λ, falls outside of the LR of the CO-side receiver. With this, the VC denotes the new reference for the received electrical spectrum and the uplink is transparently transposed to its IF < f_{UL}.

It shall be stressed that the proposed scheme does not require the provision of a RF-based LO to the EAM section, as proposed earlier for an EAM-based implementation of a photomixer [27], and can therefore omit both, mm-wave RF synthesizer and mm-wave mixer components. As we will demonstrate shortly, our scheme, which inherently filters one of the modulation sidebands through frequency-selective coherent detection, further renders the double-sideband uplink RoF transmission robust to dispersion-induced penalties.

C. Full-Duplex RoF on Single Physical-Layer Resource

Apart from the frequency translation of radio signals, a third challenge resides in finding an efficient method to support full-duplex transmission. For this purpose, the optical transmission layer is required to dedicate additional physical-layer resources to accomplish cross-talk free bidirectional RoF transmission, for which the arguably simplest way is the adoption of WDM technology [28-30]. However, besides moving to a paired optical spectrum that is characterized by dedicated wavelengths for down- and uplink, the component count at the cost-sensitive RRH is doubled, too. Even though the first aspect could be addressed through orthogonal modulation to re-use a single wavelength [31], it is still required to have dedicated opto-electronic converters for sustaining simultaneous downlink reception and upstream transmission at the RRH.

Collapsing these function in a multi-functional photonic device has been investigated in a few earlier works [32-35], primarily focusing on the EAM and its offerings as highly-efficient intensity modulator and fast photodiode, respectively. Since, however, the received downlink features a signal level that differs by ~7 orders-of-magnitude when compared to the much stronger uplink, a cross-talk robust duplex scheme is paramount. This can be either found with time division

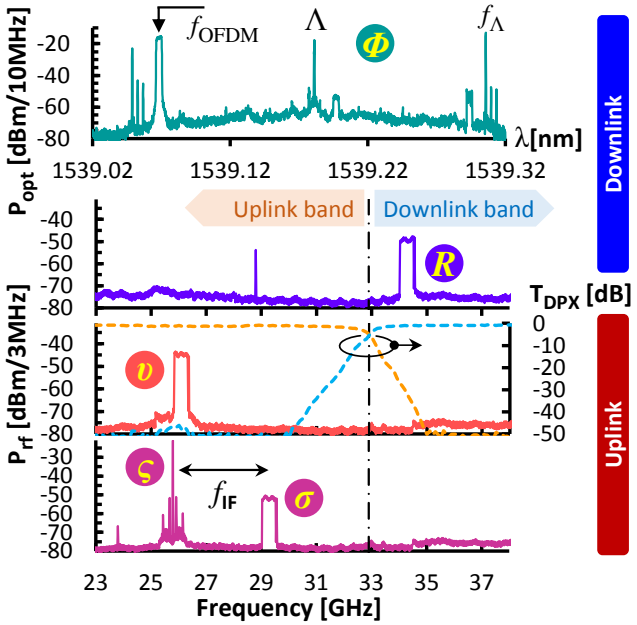

Fig. 5. Transmitted downlink signal spectra.

duplexing (TDD) [34], or by introducing frequency division duplexing (FDD) as a way to migrate from a paired optical spectrum to a paired RF configuration [32, 35]. Figure 3 highlights this challenge of simultaneous uplink transmission, which generates a substantial amount of cross-talk χ in the vicinity of the downlink at f_{DL}.

The experiment in this work will demonstrate, for the first time, full-duplex RoF transmission over a single EML with radio signals allocated to a mm-wave band.

III. Experimental Setup

Figure 4 presents our experimental setup. At the CO, we used two schemes for downlink radio signal transmission, relying on *(i)* RF-based up-conversion to a mm-wave carrier in the K_a-band (*δ* in Fig. 4) and *(ii)* photonic up-conversion (*Φ*) through independent sideband modulation. The first scheme modulates the downlink signal on an optical carrier Λ, using a Mach-Zehnder modulator (MZM). A 50/100 GHz interleaver (IL) is

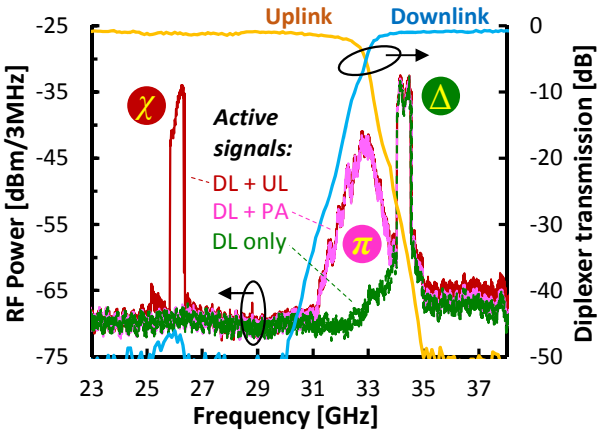

Fig. 6. Received RF spectra at the downlink RRH branch.

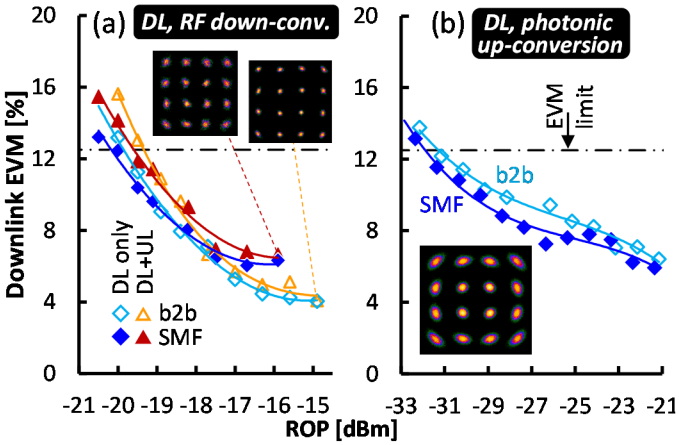

Fig. 7. Downlink radio-over-fiber transmission performance employing (a) RF-based and (b) photonic up-conversion.

inserted to obtain optical single-sideband (SSB) transmission for the already up-converted downlink RoF signal. This mitigates dispersion-induced signal fading during photodetection at the RRH. The second scheme independently modulates the two sidebands of a suppressed optical carrier Λ with the downlink radio signal at f_{OFDM} and a pilot tone f_Λ, respectively. This is accomplished through an I/Q modulator, as described in [11]. By replacing the optical carrier Λ by the pilot tone that serves as VC to lock the RRH transceiver, the mm-wave signal is established at a RF carrier frequency that resembles the sum of frequencies $f_{OFDM} + f_\Lambda$.

The transmitted mm-wave signal spectra are reported in Fig. 5. The downlink spectrum intended for photonic up-conversion (Φ) was captured with a high-resolution optical spectrum analyzer. It shows the independently modulated downlink sidebands with the VC at f_Λ = 15.75 GHz and the OFDM signal at f_{OFDM} = 14.25 GHz, both referenced to the suppressed optical carrier Λ at 1539.2 nm. The optical carrier Λ was suppressed by the I/Q modulator by 20.5 dB for optimally set modulator biases. Further shown are the RF up-converted downlink signal (R) at 34.3 GHz with a corresponding uplink signal (υ) at 26.1 GHz. To prove the concept of photonic down-conversion, we use a modified uplink signal for which we append a VC (ς) at 25.8 GHz at a power of +8 dB relative to the OFDM signal (σ), which is now centered at 29.3 GHz. With this configuration, the photonic down-conversion process will transpose the uplink OFDM signal to an IF carrier at f_{IF} = 3.5 GHz while we further ensure that the VC is sufficiently strong to lock the EML, as will be proven shortly. Several OFDM signals had 128 sub-carriers that span over a RF bandwidth of 500 MHz. These sub-carriers were independently loaded with 16-QAM.

We then launch the downlink to a filterless optical distribution network (ODN). The fronthaul network is composed by a dual-fiber feeder with a length of 14.3 km and a shorter 1-km single-mode fiber (SMF) drop segment. A circulator resembles the directional split at the optical domain.

Our simplified RRH builds on an EML as only opto-electronic converter between the optical layer and the mm-wave RF band. It simultaneously detects the downlink while transmitting the uplink, as described earlier. The directional split in the RF domain is accomplished through a mm-wave diplexer (DPX), whose transmission function is included in Fig. 5. It has a cross-over frequency of 32.9 GHz that defines the down- and uplink sub-bands to implement a paired RF spectrum within the K_a-band.

The employed EML is a butterfly-packaged device (see inset of Fig. 4) with a 3-dB bandwidth of 33 GHz. The EAM section is biased at -1.2V, which falls to an intermediate value between transparency and high extinction. We optimized the input state of polarization for the received downlink signal with a manual polarization controller (PC, ξ in Fig. 4). A diversity detector architecture such as demonstrated in [36] can be employed to mitigate polarization control, but was not pursued in this work. Moreover, the isolator inside the butterfly packaged prevents an efficient detection of the downlink due to its isolation of 35.2 dB, as characterized following the method in [23]. For the downlink signal, this reversely passed isolator means a highly increased optical budget at the input of the RRH. To offset this unintended excursion in optical budget between CO transmitter and RRH detector, we have extraordinarily employed an EDFA in the downlink feeder of the ODN (ε) to overcome this reverse isolator loss. The received power, to which several performance measurements will be related, is then referred to the optical power level after having passed the isolator reversely, at the input of the EAM section (see ROP_{DL} in Fig. 4). In a practical deployment scenario, where an EML would be used without this co-packaged isolator, this EDFA could be omitted. In addition, the circulator at the ODN with preceding variable optical attenuator (VOA) would likely be replaced by a 2×N tree splitter.

At the mobile equipment (ME), the downlink at the higher K_a-band and the uplink in the lower K_a-band are down- and up-converted, respectively, employing RF-based mixers. We have omitted a wireless channel between the RRH and the ME to focus our attention exclusively on penalties arising at the optical-layer transmission of the RoF signals and the photonic up- and down-conversion techniques employed at the head- and tail-end of the fronthaul link.

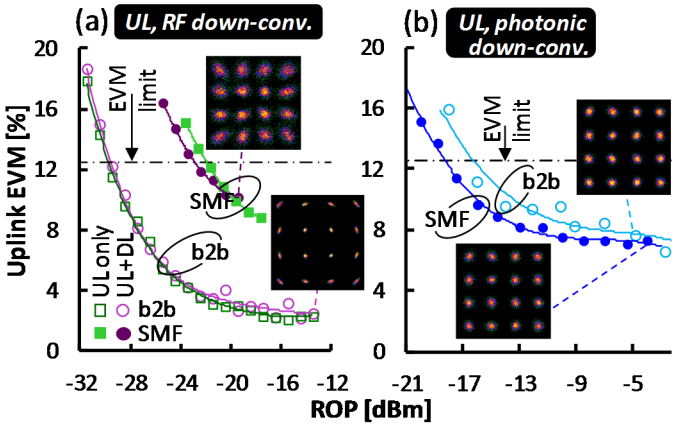

Fig. 8. Uplink radio-over-fiber transmission performance employing (a) RF-based and (b) photonic down-conversion.

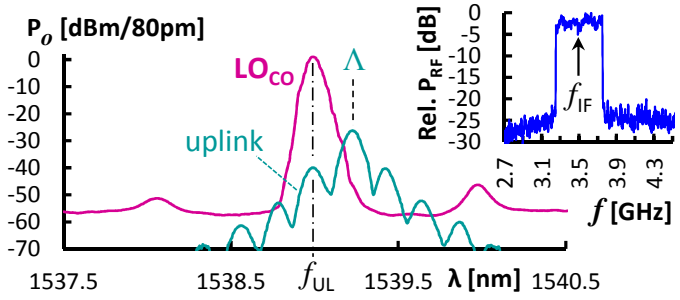

Fig. 9. Uplink spectra in case of photonic down-conversion.

We employed an optically preamplified direct-detection PIN receiver with subsequent RF down-converter at the uplink branch of the CO. A semiconductor optical amplifier (SOA) with a small-signal gain of 19.6 dB at 1540 nm and a noise figure of 6.7 dB was used as preamplifier. This traditional receiver is benchmarked against an EML-based coherent receiver providing the required means for photonic down-conversion. Again, we used a preceding EDFA to offset the reverse isolator loss of the butterfly EML at the CO receiver.

IV. Results and Discussion

A. Full-Duplex Signal Crosstalk

Figure 6 reports the received RF signal spectra at the downlink branch of the RRH (δ in Fig. 4) under various conditions, together with the two transmission windows T_{DPX} of the mm-wave diplexer. These spectra are reported for a downlink ROP of -16 dBm. Without activated uplink branch, the downlink signal Δ at 34.3 GHz features a good signal-to-noise ratio after coherent optical signal reception of this analogue RoF signal by the EML. When activating the uplink power amplifier (PA) at the diplexer input (Π in Fig. 4), yet without applying an uplink OFDM signal, we see the background noise π of the PA arising at the cross-over point between the up- and downlink bands. This reflects the large dynamic range in down- and uplink power levels at the directional split within the RRH. When applying the uplink radio signal at 26.1 GHz, we can clearly see its crosstalk note χ (see Fig. 3 as a reference) in the downlink branch of the RRH, which is determined by the set EAM drive for the uplink and thus independent of the link conditions. Still, this crosstalk is well suppressed by the high rejection of >40 dB of the diplexer, resulting in a marginally elevated noise background at the downlink band and, more importantly, a residual uplink power level that is similar to that of the downlink. The latter permits a data acquisition without dynamic range limitations at the analogue-to-digital converter that acquires the downlink signal.

B. Downlink Transmission Performance

We have firstly assessed the performance of the downlink with RF-based up-conversion to the K_a-band as a function of the ROP for half- and full-duplex transmission, in a back-to-back (b2b) scenario and with fiber-based ODN. The corresponding error vector magnitude (EVM) is reported in Fig. 7(a). We obtain a low EVM of 4.1% for half-duplex back-to-back transmission without present uplink signal (◇). The clean 16-QAM OFDM constellation proves the good signal integrity despite relying on a low-complexity analogue coherent homodyne detection method, which supports an excellent frequency and phase stability during opto-electronic signal conversion of the mm-wave signal at the RRH. The EVM antenna limit at 12.5% for 16-QAM is surpassed at a ROP of -19.8 dBm. In case of full-duplex transmission with activated uplink signal (△), we see a marginal EVM increase of 0.5% at high ROP. At the same time, the sensitivity at the EVM limit degrades by 0.4 dB. These small penalties confirm the excellent uplink rejection at the directional split point of the RRH, rendering FDD as a cross-talk robust duplexing method. Moreover, we obtain a similar sensitivity as in the back-to-back case with a fiber-populated ODN (◆,▲). This is linked to the optical single-sideband launch at the CO transmitter to mitigate dispersion-induced fading. Even though the EVM at higher ROP levels worsens to 6.1%, it still falls well below the antenna limit of 12.5%.

C. Photonic Up-Conversion of mm-Wave Downlink

Figure 7(b) reports the downlink EVM when the RRH transceiver is locked to the VC at f_Λ to photonically up-convert the downlink OFDM signal from f_{OFDM} = 14.25 GHz to f_{DL} = 30 GHz. As a result of limitations in the AWG sampling rate of 32.5 GSa/s when driving the I/Q modulator at the CO, this mm-wave carrier frequency falls below the cross-over frequency of the DPX and therefore into the uplink band defined earlier. We therefore took out the DPX and performed half-duplex downlink measurements to prove the concept of locking the RRH transceiver on a VC embedded with the downlink. For the back-to-back downlink transmission, we obtained a sensitivity of -31.3 dBm at the EVM limit (◇). The improvement in sensitivity when compared to the RF-based up-conversion (Fig. 7(a)) is explained by the suppression of the powerful optical carrier Λ, which by itself does not include downlink information and can be therefore substituted by a weaker VC due to coherent reception at the RRH. Furthermore, we do not see a penalty for transmission over a fiber-furnished ODN (◆).

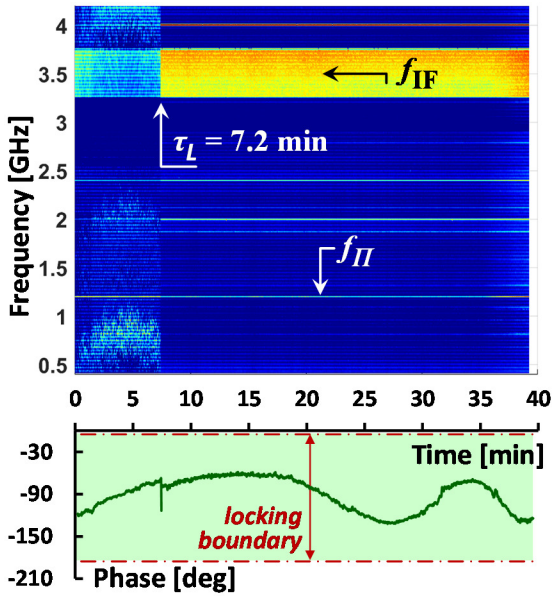

Fig. 10. Stability of the EML receiver when locked on a VC.

D. Uplink Transmission Performance

Figure 8(a) presents the uplink EVM for direct detection using the SOA+PIN receiver and RF-based down-conversion. We accomplish a low EVM of 2.2% for back-to-back transmission in half-duplex (□) and full-duplex (○) modes when a downlink signal is present. The sensitivity at the antenna limit is -29.7 dBm. When populating the ODN with fiber, conditions change: Since we cannot apply an optical single-sideband filter at the RRH due to complexity considerations, dispersion-induced fading is impacting the mm-wave uplink RoF transmission, as given by the frequency response of the optical transmission fiber [37]. We see a significant sensitivity penalty of >6.8 dB at the EVM limit (●,■) and a strong increase in the minimum EVM that can be achieved, which rises to 8.8%.

E. Photonic Down-Conversion of mm-Wave Uplink

Photonic down-conversion at the EML-based coherent homodyne uplink receiver of the CO can mitigate this penalty as it selects only one of the modulation sidebands while it translates the mm-wave uplink signal to an IF in the sub-6GHz range. Figure 9 presents the spectral configuration for this process. The LO of the EML receiver at the CO is centered on the lower mm-wave modulation sideband of the uplink signal that is spaced by f_{UL} from the optical carrier Λ. The EML is then optically locked on the VC that has been appended to the uplink OFDM signal (see ς in Fig. 5). This yields the down-converted OFDM signal at f_{IF} = 3.5 GHz, as reported in Fig. 9.

The corresponding EVM performance, shown in Fig. 8(b), proves the point of a dispersion-tolerant uplink RoF transmission. The back-to-back reception sensitivity is -16.2 dBm at the EVM antenna limit (○). Together with the uplink launch of 2.5 dBm from the RRH, this defines the maximum optical budget of 18.7 dB for the ODN. Further improvement can be expected for chip-based EML implementations without co-packaged isolator. More importantly, the dispersion-induced penalty inherent to direct-detection based uplink reception has been fully recovered (●). The clean 16-QAM OFDM constellations prove the excellent signal integrity after optical frequency translation due to joint (*i*) coherent homodyne detection and (*ii*) photonic down-conversion of the mm-wave OFDM signal to an IF of 3.5 GHz, without requiring either RF mixer or mm-wave synthesizer.

Finally, we investigated the durability of the LO locking on the VC by appending an auxiliary pilot tone at f_{Π} = 1.2 GHz to track its RF phase, which serves as a performance indicator for the locking stability. Given that correct locking is accomplished, the VC will fall at f = 0, while the transmitted pilot frequency f_{Π} is not subject to frequency shifting. Moreover, the same pilot tone is weakly reflected at the front facet of the EML and can be therefore detected together with the emitted optical LO of the EML at a PIN receiver (μ in Fig. 4). The resulting beat note at f_{Π} can then be phase-discriminated with an auxiliary RF-based LO matched to f_{Π}. This yields the optical phase of the EML emission, which is determined by the relative mismatch between the free-running EML and input signal wavelengths [38]. It can be directly acquired and used as a feedback to tune the DFB section of the EML as LO for the down-converter by simply adjusting the DFB bias current [39].

Figure 10 presents the spectrogram of the received RF signal spectrum after down-conversion for an acquisition time of more than 30 min, together with the RF phase of the pilot tone. We see that once the EML is locked on the received radio signal, which occurs at τ_L = 7.2 min, a stable condition is obtained even without closed-loop control. The OFDM signal can be clearly discerned at f_{IF} = 3.5 GHz. Moreover, the pilot phase remains within a peak-to-peak deviation of 74°, which is attributed to the sufficiently accurate temperature control of the EML receiver. This swing in pilot phase, which is well below a relative ±90° range, indicates that stable locking is accomplished since the received VC remains within the locking range of the LO, despite any residual fluctuations in laser emission frequencies at RRH and CO.

V. Conclusion

We have demonstrated the full-duplex transmission of analogue mm-wave radio signals at 34.3/29.3 GHz over an optical budget of 18.7 dB and a reach of 15 km, while proving the good signal integrity and a low EVM for OFDM radio signals in combination with EML-based transceiver optics at the RRH. We further showed the beneficial use of coherent EML technology to accomplish a highly simplified and radio-transparent photonic up- and down-conversion for the downlink and uplink signal, respectively. Scaling up to even higher RF windows beyond the K_a-band mm-wave region would require high-bandwidth EAMs, as it is available for up to 100 GHz. RoF transmission over a filterless ODN, as enabled through simplified coherent reception at the RRH, further permits a smooth wireline-wireless integration in brown-field, splitter-based fiber plants.

REFERENCES

[1] S. Zhang, C. Xiang, and S. Xu, "6G: Connecting Everything by 1000 Times Price Reduction," *IEEE Open J. of Vehicular Technol.*, vol. 1, pp. 107-115, Mar. 2020.

[2] A. de la Oliva, J.A. Hernandez, D. Larrabeiti, and A. Azcorra, "An overview of the CPRI specification and its application to C-RAN-based LTE scenarios", *IEEE Comm. Mag.*, vol. 54, no. 2, pp. 152-159, Feb. 2016.

[3] K. Mallick *et al.*, "Bidirectional OFDM-MMWOF transport system based on mixed QAM modulation format using dual mode colorless laser diode and RSOA for next generation 5-G based network," *Opt. Fib. Technol.*, vol. 64, art. no. 102562, Jul. 2021.

[4] K. Mallick *et al.*, "Bidirectional OFDM Based MMW/THzW Over Fiber System for Next Generation Communication," *Phot. J.*, vol. 13, no. 4, art. no. 7301207, Aug. 2021.

[5] R. Mukherjee, K. Mallick, P. Mandal, B. Dutta, B. Kuiri, and A. S. Patra "Bidirectional hybrid OFDM based free-space/wireless-over-fiber transport system," *Optical and Quantum Electronics*, vol. 52, art. no. 311, Jun. 2020.

[6] A. Udalcovs *et al.*, "Total Cost of Ownership of Digital vs. Analog Radio-Over-Fiber Architectures for 5G Fronthauling," *IEEE Access*, vol. 8, pp. 223562-223573, Dec. 2020.

[7] B. Schrenk, A. Val Marti, T. Zemen, and F. Karinou, "Full-Duplex Coherent Analogue mm-wave RoF Transmission with Simplified RRH and Photonic Down-Conversion of Uplink", in *Proc. Europ. Conf. Opt. Comm. (ECOC)*, Glasgow, United Kingdom, Oct. 2023, paper Tu.B.4.4.

[8] K. Li, and J. Yu, "Photonics-Aided Terahertz-Wave Wireless Communication," *J. Lightwave Technol.*, vol. 40, no. 13, pp. 4186-4195, Dec. 2022.

[9] S. Yu, W. Gu, A. Yang, T. Jiang, and C. Wang, "A Frequency Quadrupling Optical mm-Wave Generation for Hybrid Fiber-Wireless Systems," *J. Sel. Areas of Comm.*, vol. 31, no. 12, pp. 797-803, Dec. 2013.

[10] Z. Xu, X. Zhang, and J. Yu, "Frequency upconversion of multiple RF signals using optical carrier suppression for radio over fiber downlinks," *Opt. Expr.*, vol. 15, no. 25, pp. 16737-16747, Dec. 2007.

[11] A. Val Marti, N. Vokic, T. Zemen, and B. Schrenk, "Hybrid CAP / mm-wave OFDM Vector Modulation for Photonic Frequency Conversion in a Single-Sideband Feeder", in *Proc. Opt. Fib. Comm. Conf. (OFC)*, San Diego, United States, Mar. 2022, paper Th1I.3.

[12] L. Gonzalez-Guerrero, M. Ali, R. Guzman, H. Lamela, and G. Carpintero, "Photonic Sub-Terahertz IM Links: Comparison Between Double and Single Carrier Modulation," *J. Lightwave Technol.*, vol. 40, no. 18, pp. 6064-6070, Sep. 2022.

[13] K. Zeb *et al.*, "Broadband Optical Heterodyne Millimeter-Wave-over-Fiber Wireless Links Based on a Quantum Dash Dual-Wavelength DFB Laser," *J. Lightwave Technol.*, vol. 40, no. 12, pp. 3698-3708, Feb. 2022.

[14] S.R. Moon, M. Sung, J.K. Lee, and S.H. Cho, "Cost-Effective Photonics-Based THz Wireless Transmission Using PAM-N Signals in the 0.3 THz Band," *J. Lightwave Technol.*, vol. 39, no. 2, pp. 357-362, Jan. 2021.

[15] C. Wang, J. Yu, X. Li, P. Gou, and W. Zhou, "Fiber-THz-Fiber Link for THz Signal Transmission," *Phot. J.*, vol. 10, no. 2, art. no. 7200706, Apr. 2018.

[16] W. Li *et al.*, "Photonics-assisted 320 GHz THz-band 50 Gbit/s Signal Outdoor Wireless Communication over 850 Meters", in *Proc. Opt. Fib. Comm. Conf. (OFC)*, San Diego, United States, Mar. 2023, paper Th4C.5.

[17] L. Zhao, K. Wang, and W. Zhou, "Transmission of 4096-QAM OFDM at D-band," *Opt. Expr.*, vol. 31, no. 2, pp. 2270-2281, Jan. 2023.

[18] Y. Cai *et al.*, "Real-time 100-GbE fiber-wireless seamless integration system using an electromagnetic dual-polarized single-input single-output wireless link at W band," *Opt. Lett.*, vol. 48, no. 4, pp. 928-931, 2023.

[19] J. Zhang *et al.*, "Real-time demonstration of 103.125-Gbps fiber–THz–fiber 2×2 MIMO transparent transmission at 360-430 GHz based on photonics," *Opt. Lett.*, vol. 47, no. 5, pp. 1214-1217, 2022.

[20] W. Wang *et al.*, "Optical polarization division multiplexing fiber-wireless integration system at K_a-band based on a low-cost dual-drive MZM," *Opt. Expr.*, vol. 29, no. 23, pp. 37453-37463, Nov. 2021.

[21] B. Schrenk, "The Electroabsorption-Modulated Laser as Optical Transmitter and Receiver: Status and Opportunities", *IET Optoelectronics*, vol. 14, no. 6, pp. 374-385, Dec. 2020.

[22] L. Yu *et al.*, "A Widely Tunable Directly Modulated DBR Laser With High Linearity," *Phot. J.*, vol. 6, no. 4, art. no. 1501308, Aug. 2004.

[23] B. Schrenk, M. Hofer, and T. Zemen, "Analogue Receiver for Coherent Optical Analogue Radio-over-Fiber Transmission," *Opt. Lett.*, vol. 42, no. 16, pp. 3165-3168, 2017.

[24] S. Zhu, X. Fan, M. Li, N. H. Zhu, and W. Li, "Microwave photonic frequency down-conversion and channel switching for satellite communication," *Opt. Lett.*, vol. 45, no. 18, pp. 5000-5003, 2020.

[25] N.P. O'Malley *et al.*, "Architecture for integrated RF photonic downconversion of electronic signals," *Opt. Lett.*, vol. 48, no. 1, pp. 159-162, 2023.

[26] D. Wang, F. Yang, Y. Wang, Z. Chen, D. Yang and F. Wu, "Filter-Free Photonic Image-Rejection Down-Conversion for Distributed Antenna Applications," *Phot. J.*, vol. 13, no. 2, pp. 1-10, Apr. 2021.

[27] D.S. Shin *et al.*, "Optoelectronic RF Signal Mixing Using an Electroabsorption Waveguide as an Integrated Photodetector/Mixer," *Photon. Technol. Lett.*, vol. 12, no. 2, pp. 193-195, Feb. 2000.

[28] D.N. Nguyen *et al.*, "Full-duplex transmission of multi-Gb/s subcarrier multiplexing and 5G NR signals in 39 GHz band over fiber and space," *Appl. Opt.*, vol. 61, no. 5, pp. 1183-1193, Feb. 2022.

[29] J. Kim *et al.*, "MIMO-Supporting Radio-Over-Fiber System and its Application in mmWave-Based Indoor 5G Mobile Network," *J. Lightwave Technol.*, vol. 38, no. 1, pp. 101-111, Jan. 2020.

[30] L. Bogaert *et al.*, "SiPhotonics/GaAs 28-GHz Transceiver With Reflective EAM for Laser-Less mmWave-Over-Fiber," *J. Lightwave Technol.*, vol. 39, no. 3, pp. 779-786, Feb. 2021.

[31] B. Wenlin *et al.*, "A WDM-PON compatible wavelength-reused bidirectional in-band full-duplex radio-over-fiber system," *Opt. Communications*, vol. 463, p. 125408, 2020.

[32] A. Stöhr, K. Kitayama, and D. Jäger, "Full-Duplex Fibre-Optic RF Subcarrier Transmission Using a Dual-Function Modulator/Photodetector," *IEEE Trans. Microw. Theory and Tech.*, vol. 47, no. 7, pp. 1338-1341, Jul. 1999.

[33] R.B. Welstand, S.A. Pappert, C.K. Sun, J.T. Zhu, Y.Z. Liu, and P.K.L. Yu, "Dual-function electroabsorption waveguide modulator/detector for optoelectronic transceiver applications," *Photon. Technol. Lett.*, vol. 8, no. 11, pp. 1540-1542, Nov. 1996.

[34] M.P. Thakur *et al.*, "480-Mbps, Bi-Directional, Ultra-Wideband Radio-Over-Fibre Transmission Using a 1308/1564-nm Reflective Electro-Absorption Transducer and Commercially Available VCSELs," *J. Lightwave Technol.*, vol. 27, no. 3, pp. 266-272, Feb. 2009.

[35] B. Schrenk, "The EML as Analogue Radio-over-Fiber Transceiver – a Coherent Homodyne Approach," *J. Lightwave Technol.*, vol. 37, no. 12, pp. 2866-2872, Jun. 2019.

[36] B. Schrenk, and F. Karinou, "Simple Laser Transmitter Pair as Polarization-Independent Coherent Homodyne Detector," *Opt. Expr.*, vol. 27, no. 10, pp. 13942-13950, 2019.

[37] F. Ramos, and J. Marti, "Frequency Transfer Function of Dispersive and Nonlinear Single-Mode Optical Fibers in Microwave Optical Systems," *Phot. Technol. Lett.*, vol. 12, no. 5, pp. 549-551, May 2000.

[38] F. Mogensen, H. Olesen, and G. Jacobsen, "Locking Conditions and Stability Properties for Semiconductor Laser with External Light Injection," *Journal Quantum Electron.*, vol. 21, no. 7, pp. 784-793, Jul. 1985.

[39] Z. Liu, and R. Slavík, "Optical Injection Locking: From Principle to Applications," *J. Lightwave Technol.*, vol. 38, no. 1, pp. 43-59, 2020.